FMDB *Transactions on Sustainable Applied Sciences*

Enhanced Ferroelectric and Piezoelectric Properties in $NaNbO_3$-based Materials via BiGd/$YKZrTiO_3$ Two-Step Sintering

P. Elaiyaraja[1, *], Narasimha Rao Boinapalli[2]

[1]Department of Physics, SRM Institute of Science and Technology, Ramapuram, Chennai, Tamil Nadu, India.
[2]Department of Data and Analytics (D&A), Weisiger Group, Charlotte, North Carolina, United States of America.
elaiyarajaphysics@gmail.com[1], nara.boinapalli@gmail.com[2]

Abstract: The new ceramic composites are 0.98 ($NaNbO_3$)-0.02 Bi0.45Gd0.05K0.5Zr0.7Ti0.3O3 and 0.85 ($NaNbO_3$)-0.15 Bi0.45Y0.04K0.5Zr0.7Ti0.3O3. Lead-free and polycrystalline were created using the traditional solid-state technique and have been widely researched for their various applications. Their manufacturing was accomplished through the use of a two-step sintering method. A perovskite structure with a Pmc21 space group was discovered to be present in the material when it was subjected to analysis. This was accomplished by utilising Schecher's formula and Williamson-Hall plots derived from XRD spectra in order to determine the particle size and strain. According to the results of the Raman spectroscopy, the vibrational spectral lines have shifted to a lower frequency, with the frequency range falling between 100 and 800 cm-1. Furthermore, the grain morphology was clearly characterised and varied in the FE-SEM pictures which were obtained. Band structure values were observed in the UV-Vis spectrum, and they ranged from 3.2 eV to 2.8 eV. There were emission bands in the green (522 nm), yellow (575 nm), and red (693 nm) ranges that were observed in the photoluminescence spectrum. The data from the dielectric material demonstrated a decrease in symmetry at temperatures ranging from 10 kHz to 1 MHz. In addition, the ferroelectric and piezoelectric coefficients were improved as a result of increasing doping, with d33 values of 150 (pc/N) and 255 (pc/N) respectively.

Keywords: UV Spectrometers; Raman Spectroscopy; Dielectric Constant; Analysis of the Emission Spectrum; Ferroelectric and Piezoelectric; Field Emission Scanning Electron Microscope (FE-SEM); Two-Step Sintering.

Received on: 03/11/2023, **Revised on:** 26/12/2023, **Accepted on:** 14/02/2024, **Published on:** 03/06/2024

Journal Homepage: https://www.fmdbpub.com/user/journals/details/FTSASS

DOI: https://doi.org/10.69888/FTSASS.2024.000163

Cite as: P. Elaiyaraja and N. R. Boinapalli, "Enhanced Ferroelectric and Piezoelectric Properties in $NaNbO_3$-based Materials via BiGd/$YKZrTiO_3$ Two-Step Sintering," *FMDB Transactions on Sustainable Applied Sciences*., vol.1, no.1, pp. 10–20, 2024.

1. Introduction

India Lead-based compounds, like $PbTiO_3$, $Pb(Zr_{0.7}Sn_{0.3})$ TiO_3 and $Pb_{0.92}La_{0.08}TiO_3$, are great at piezoelectricity but are very bad for the environment and your health [1]-[3]. Some compounds that don't contain lead, such as $KNaLiNbTaO_3$-$CaZrO_3$, $KNaNbSbO_3$, $KNaNbO_3$, $NaBiBaTiO_3$ and $NaNbO_3$ could be used in electrical applications [4]-[6]. However, these materials have weak thermal stability and low density. Many investigations are ongoing to improve these properties, potentially replacing lead-based materials in various applications while reducing environmental impact and health risks. The development of lead-free piezoelectric materials has the potential to improve technology and sustainability in several applications significantly.

*Corresponding author.

Among these materials, $NaNbO_3$ has shown good piezoelectric characteristics and thermal stability. Researchers are always looking for methods to enhance the performance of $NaNbO_3$ and other lead-free materials, making them viable options for various electrical and sensor applications [7]. By successfully developing and commercializing these materials, the industry may transition to a more sustainable and ecologically friendly future, eliminating its dependence on harmful lead-based products. These advances in materials science help the environment and provide new opportunities for innovation in electrical gadgets. $NaNbO_3$ and other lead-free materials can perform well, if not better, than conventional choices, allowing the industry to fulfil the rising need for sustainable technological solutions. Companies that research and develop these materials may remain ahead of the competition and contribute to a cleaner, greener future for everybody.

Researchers use a three-step sintering procedure to improve the performance and quality of lead-free piezoelectric materials. This method increases the materials' performance and electrical characteristics, making them more environmentally friendly and suitable for sensors, actuators, and energy harvesting systems. Traditional sintering processes have limitations when creating ceramics with submicron grain sizes. Researchers are exploring alternative methods like pressure-assisted sintering, spark plasma sintering (SPS), and pulsed electric current sintering (PECS) to address this. These methods provide more precise control over grain size and distribution, improving lead-free piezoelectric materials' performance [8]-[9]. Many lead-free piezoelectric materials function well during the phase transition from rhombohedral to tetragonal (R-T). Ti and Zr doped materials have been demonstrated to greatly enhance piezoelectric performance, making them suited for advanced technological applications [10]. Researchers may modify doping levels and manufacturing techniques to tailor materials to specific performance requirements, opening new avenues for cutting-edge electronics. Lead-free piezoelectric materials can transform sectors including healthcare, telecommunications and renewable energy.

Adding rare-earth elements to $NaNbO_3$ (Bi, K, Ti, and Zr) has shown promise for increasing its piezoelectric capabilities, resulting in more efficient and long-lasting electrical systems [11]. With ongoing research and development, the future of lead-free piezoelectric materials is bright, with endless possibilities for widespread use in various industries. These advancements can potentially revolutionize the design and manufacture of medical devices, making them more sensitive and durable. In the telecommunications industry, lead-free piezoelectric materials may help to create smaller, more efficient components for smartphones and other devices. Furthermore, these materials may improve the efficiency of solar panels and other energy-collecting devices in the renewable energy business. Lead-free piezoelectric materials have several applications, making them a top priority for researchers and engineers.

New research used a solid-state technique to develop novel piezoelectric materials: 0.98 ($NaNbO_3$)-$0.02Bi_{0.45}Gd_{0.05}K_{0.5}Zr_{0.7}Ti_{0.3}O_3$ and 0.85 ($NaNbO_3$)-0.15 $Bi_{0.45}Y_{0.04}K_{0.5}Zr_{0.7}Ti_{0.3}O_3$. These materials show exceptional ferroelectric and piezoelectric properties, especially when doped with Y/Gd elements. These materials may be used in electrical and optical applications, and when mixed with rare earth and bismuth oxides, they can generate light via a "lattice-sensitized" process.

2. Experimental

A Two-step sintering process was used to make the new lead-free ceramic samples of 0.98 ($NaNbO_3$)-$0.02Bi_{0.45}Gd_{0.05}K_{0.5}Zr_{0.7}Ti_{0.3}O_3$ and 0.85 ($NaNbO_3$)-0.15 $Bi_{0.45}Y_{0.04}K_{0.5}Zr_{0.7}Ti_{0.3}O_3$ solid solution materials. The materials, including Na_2CO_3, Nb_2O_5, Bi_2O_3, Y_2O_3/Gd_2O_3, K_2CO_3, TiO_2 and ZrO_2 were dried at 150 °C due to their complexity and ionic radius. After stoichiometric weighing, the raw components were combined, requiring three hours of hand grinding. The powders that had been dried were then crushed before being put through two rounds of calcination at temperatures of 850 degrees Celsius and 900 degrees Celsius for three hours each. Pellets with a diameter of ten millimetres and a thickness of one millimetre were produced by combining the calcined powders with polyvinyl alcohol (PVA), milling them for an extra hour, and then pressing them under five tonnes of pressure.

Following a two-step sintering process, the PVA was removed by baking at temperatures of 1200 degrees Celsius for one hour and 1100 degrees Celsius for three hours. Additionally, a silver conductive paste was put to both sides of the surface, and then it was baked at a temperature of 600 degrees Celsius for 10 minutes. The ceramics were subjected to tests of their piezoelectric characteristics before the piezoelectric capabilities of the pellets were evaluated. The pellets were placed in a silicon oil bath at a temperature of 150 degrees Celsius for three hours (at a voltage of 2–5 kilovolts per square centimetre). The crystalline structure of the ceramics was meticulously analyzed using a Bruker Instrument X-ray diffractometer, employing CuKα radiation with a wavelength of 1.5406 Å. This analysis provided critical insights into the material's crystal structure and phase composition. The Raman spectra, which were essential for investigating the vibrational modes of the ceramics, were generated using an Ar-ion laser operating at a wavelength of 488 nm. These spectra were recorded using a micro-Raman spectrometer, specifically the LabRam HR model, manufactured by M/s Horiba Jobin Yvon, which is known for its high resolution and precision in capturing Raman shifts.

To further investigate the surface morphology and elemental distribution within the ceramics, a field emission scanning electron microscope (FE-SEM) was employed. The FE-SEM used was the Sigma model from M/s Zeiss, which is renowned for its high-resolution imaging capabilities. Complementary to this, an energy-dispersive spectroscopy (EDS) system, also from M/s Zeiss, was used to analyze the elemental composition and the distribution of dopants across the ceramic surfaces. This combination of FE-SEM and EDS provided a comprehensive understanding of the microstructural features and the effectiveness of the doping process. For the optical properties, particularly the study of optical absorption, a UV-visible absorption spectrophotometer (UV 2450), manufactured by Shimadzu Corporation, was utilized. This instrument allowed for precise measurement of the absorption spectra, which is crucial for determining the band gap and understanding the electronic transitions within the ceramic materials. Each of these advanced characterization techniques contributed significantly to the detailed analysis of the ceramics, offering a robust understanding of their structural, optical, and compositional properties.

We also utilised an LCR metre manufactured by Newton 4th Instruments in order to investigate the relationship between temperature and the dielectric constant and dielectric loss of the ceramics that were coated with silver paste. The frequency ranges that were investigated were from 100 Hz to 1 MHz. To determine the piezoelectricity of the ceramic pellets, they were subjected to a DC field and immersed in a silicone oil bath at a temperature of 150 degrees Celsius. In order to evaluate the ceramic material, a ferroelectric analyzer designed by M/s Radiant Technologies and referred to as the Precise LCII 10 kV HVI-SC was utilised. In order to determine the piezoelectric properties, a piezo-d33meter, also known as a Sinocera-d33, was utilised.

3. Objective

The new lead-free and polycrystalline ceramic composites, 0.98 ($NaNbO_3$)-0.02 $Bi_{0.45}Gd_{0.05}K_{0.5}Zr_{0.7}Ti_{0.3}O_3$ and 0.85 ($NaNbO_3$)-0.15 $Bi_{0.45}Y_{0.04}K_{0.5}Zr_{0.7}Ti_{0.3}O_3$ were created using a traditional solid-state technique and have shown promise for various applications. The two-step sintering process employed in the production of the materials resulted in a perovskite structure with a Pmc21 space group. Analysis using XRD spectra, the Scherrer formula, and Williamson-Hall plots determined the particle size and strain, while Raman spectroscopy indicated a shift to lower frequencies in the vibrational spectral lines. Furthermore, increased Gd/Y with BiKZrTiO3 doping significantly improved the ferroelectric and piezoelectric coefficients, with d33 values reaching 150 pc/N and 255 pc/N at specified frequencies.

4. Review of literature

Haun et al. [1]'s study on the thermodynamic theory of $PbTiO_3$ offers significant insights into its behaviour under different conditions. Their research deepens our understanding of $PbTiO_3$'s characteristics, such as phase transitions, structural changes, and interaction with external factors like temperature and pressure. By exploring the thermodynamic properties, the study provides a theoretical foundation for predicting $PbTiO_3$'s behaviour in various applications, particularly ferroelectric materials. This work is crucial for advancing the design and optimization of $PbTiO_3$-based devices, contributing to the broader understanding of ferroelectric materials.

Zhang et al. [2] research highlights the pyroelectric properties of $Pb_{0.87}La_{0.02}Ba_{0.1}(Zr_{0.7}Sn_{0.3-x}Ti_x)O_3$ ceramics, indicating their potential for various applications. Their findings demonstrate the promising performance of these ceramics in energy harvesting and sensing devices. This research opens up new possibilities for utilizing pyroelectric materials in advanced technologies.

Hussin's et al. [3] study on lanthanum-doped $PbTiO_3$ and $PbZrTiO_3$ provides valuable insights for materials science, paving the way for advanced materials with tailored properties for various applications. His research highlights the potential for enhanced ferroelectric and piezoelectric properties in these materials, opening up new possibilities for use in sensors, actuators, and energy storage devices. Additionally, the findings could lead to the developing of more efficient and sustainable technologies.

Liang et al. [4] explores the impact of $CaZrO_3$ and $LiNbO_3$ on the phase transitions and piezoelectric properties of $K_{0.5}Na_{0.5}NbO_3$ lead-free ceramics. It provides insights into the potential enhancement of piezoelectric materials by adding specific compounds, potentially influencing the development of new materials.

Goh et al. [5] specifically focused on the synthesis of potassium niobate ($KNbO_3$) and sodium niobate ($NaNbO_3$) powders. The researchers likely aimed to investigate the feasibility and efficiency of hydrothermal synthesis for producing these materials, considering their potential applications in various fields such as ceramics, electronics, and energy storage.

Malic et al. [6] study found that adding TiO_2 to ceramics with (K, Na) NbO_3 base improves densification, dielectric properties and mechanical properties, making them suitable for electronics applications and optimizing fabrication processes.

Bai et al. [7], published in the Journal of the European Ceramic Society in 2017, explores the impact of $NaNbO_3$ templates on lead-free piezoelectric materials. Diabetic phase evolution with NaNbO3 templates can achieve enhanced performance in piezoelectric materials. The research by Bai and the team sheds light on the role of templates in improving the properties of BNT-based piezoelectric materials.

Researchers Nižňanský et al. [8] conduct an investigation on the high-pressure spark plasma sintering process, focusing on the impact of die/punch material combinations on the homogeneity of sample temperature. After doing the research, it was discovered that the selection of die/punch material had a considerable impact on the temperature distribution throughout the sample while it was being sintered. In addition, the findings offer useful insights that may be used to optimise processing parameters in order to achieve uniform temperature distribution and improve material attributes.

Guillon et al. [9] research on field-assisted sintering technology, specifically spark plasma sintering, provides a comprehensive analysis of its mechanisms, materials, and technology advancements, offering insights into its potential applications.

Lin et al. [10] provide valuable insights into the high rhombohedral to tetragonal phase transition temperature and electromechanical response in the ferroelectric system near the morphotropic phase boundary. Published in the Journal of the European Ceramic Society in 2019, this research contributes significantly to our understanding of the material's properties.

Elaiyaraja and Karunagaran [11], a study in the Journal of Materials Science Research reveals the orthorhombic pseudo-cubic phase transition in $NaNbO_3$-based solid solutions, revealing the complex interaction of piezoelectric and ferroelectric properties, providing insights for new materials with enhanced electromechanical properties.

Elaiyaraja and Karunagaran [12] study on $Bi_{0.46}Y_{0.04}K_{0.5}ZrO_3$ doping in lead-free $NaNbO_3$-based materials shows its potential in enhancing piezoelectric and ferroelectric properties, suggesting it could be a promising method for advanced functional materials.

Elaiyaraja and Karunagaran [13] study explores lead-free 0.98 $NaNbO_3$-0.02 $BiSmKZrO_3$'s potential for electrical and optical applications using the solid-state method, revealing promising properties that could make it a viable alternative in various technological fields.

Sudha et al. [14] explore the impact of Sm3+ and trioxotungsten doping on the structural, luminescence, and dielectric properties of a novel NBBT ceramic system for multifunctional device applications.

Hao et al [15] review of lead zirconate-based antiferroelectric materials discuss their synthesis methods, properties, applications, challenges, and future directions, highlighting the challenges in this field.

Ali et al. [16] explore the recent advancements in using HfO_2-based ferroelectric and antiferroelectric materials for energy-related applications, highlighting their potential to improve energy storage and conversion devices.

Semenov et al. [17] explore the relationship between structural parameters and electron transfer in ytterbium, lutetium, and cerium compounds with hydrocarbon monocycles. The findings offer insights into their electronic properties and potential applications in various fields, providing valuable insights into their electronic properties.

Soni and Kumar [18], "Luminescent Materials in Lighting, Display, Solar Cell, Sensing, and Biomedical Applications" offers a comprehensive overview of luminescent materials and their diverse applications, making it a valuable resource for researchers, engineers, and professionals in luminescence technology.

5. Result

XRD Structure: The XRD spectra of two ceramic samples, 0.98 ($NaNbO_3$)-0.02$Bi_{0.45}Gd_{0.05}K_{0.5}Zr_{0.7}Ti_{0.3}O_3$ and 0.85 ($NaNbO_3$)-0.15 $Bi_{0.45}Y_{0.04}K_{0.5}Zr_{0.7}Ti_{0.3}O_3$ are depicted in Figure 1 (a-b). Powder X-ray diffraction (XRD) was employed to analyze the phase stability and structural properties of the materials. The XRD patterns of the samples were refined using Maud software to enhance the accuracy of the results. The study aimed to refine the XRD patterns and investigate the structure, phase stability, lattice cell characteristics, and cell volume of the materials, as summarized in Table 1. The findings revealed an orthorhombic phase associated with the space groups Pmc21 for BiYKZrTiO3-doped materials and Pbma for BGKZrTiO3-doped materials. Importantly, no secondary or impure peaks were detected, confirming the purity of the samples. The calculated lattice cell characteristics closely matched those reported in the COD databases with IDs 1528864 and 9014531, supporting the accuracy and reliability of the structural analysis. These results underscore the structural integrity and phase stability of the ceramic materials, confirming their suitability for further applications.

The Williamson-Hall (W-H) method and providing insights into the volume-averaged crystalline size and its influence on the material's properties.

$$D = \frac{K\lambda}{\beta_D cos\theta} \quad (1)$$

If β_D is the wavelength in radians, K is the shape factor (K=0.09), 0.15406 is the wavelength size, and is the peak location in radians; the equation is: The microstrain was determined using these calculations.

$$\beta cos\theta = \frac{K\lambda}{D} + 4\varepsilon sin\theta \quad (2)$$

Table 1 reveals that the physical parameters of materials show lattice parameters, volume, strain and crystallite size. These parameters are crucial for understanding the structural properties of materials and their behaviour under different conditions. Additionally, they can provide valuable insights for optimizing material performance in various applications.

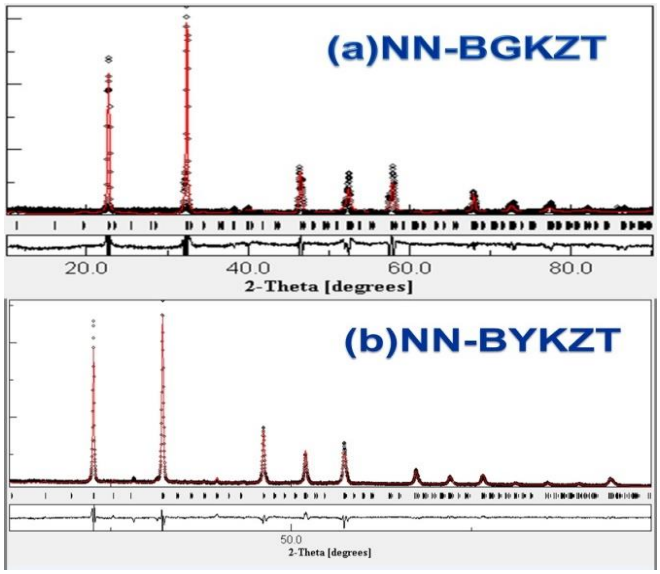

Figure 1: (a) the XRD spectrum of $BiGdKZTO_3$ Doped $NaNbO_3$ (b) the XRD spectrum of $BiYKZTO_3$ Doped $NaNbO_3$

Table 1: The structure's physical parameters

Empirical Formula	**$0.85NaNbO_3$ - $0.15BiYKZrTiO_3$**	**$0.98NaNbO_3$ - $0.02BiGdKZrTiO_3$**
Crystal system	Orthorhombic	Orthorhombic
Space group	$Pmc2_1$	Pbma:bca
a (Å)	7.8067	5.5569
b (Å)	5.5696	15.5688
c (Å)	5.5493	5.5102
Volume (Å)^3	243	476
Sig	8.0662	4.4193
Density (g/cm^3)	4.4740	4.4193
Microstrain	0.0035	0.1903
Particle Size D (nm)	55	47
Dislocation densityδ (nm)$^{-1}$	0.0004	0.00045
Strain	**0.0018**	**0.2663**

Raman spectroscopy**:** Raman spectroscopy analysis suggests that the Nb-O bond in the $NaNbO_3$ host lattice is either shortening or experiencing increased compression. This structural change is indicated by a shift in the Raman bands towards lower wave numbers, particularly at 259, 221, 184, 142, and 117 cm^{-1}. These shifts, though minor, are significant as they reflect the successful incorporation of Bi/Y and Gd/KZT ions into the $NaNbO_3$ lattice. The integration of these ions has been confirmed by the observed changes in the Raman spectrum, which also suggests that the perovskite structure remains stable and functions as intended. The successful incorporation of these ions into the lattice plays a critical role in maintaining the structural integrity of the perovskite, ensuring its ability to perform under various conditions. The shift in the Raman bands not only provides evidence of this successful doping but also offers insights into the resulting changes in the lattice dynamics and bonding environment. These findings are crucial for understanding the material's properties and potential applications, particularly in fields requiring stable and functional perovskite structures.

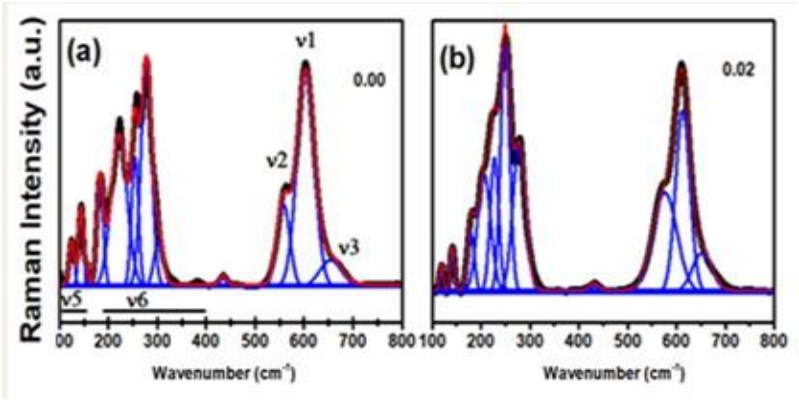

Figure 2: (a) the Raman spectrum of $BiGdKZTO_3$ Doped $NaNbO_3$ (b) the Raman spectrum of $BiYKZTO_3$ Doped $NaNbO_3$

UV spectrometers: Figure 3 displays the energy bandgap spectra of 0.98 ($NaNbO_3$)-0.02 $Bi_{0.45}Gd_{0.05}K_{0.5}Zr_{0.7}Ti_{0.3}O_3$ and 0.85 ($NaNbO_3$)-0.15 $Bi_{0.45}Y_{0.04}K_{0.5}Zr_{0.7}Ti_{0.3}O_3$ and its related solid solutions. The UV-VIS absorption spectra were utilized to acquire the absorption data, which was then used to calculate the Wood-Tac equation. The absorption coefficient and band gap are interconnected and can be expressed as:"

$$\alpha h\upsilon = B(h\upsilon - E_g)^n \qquad (3)$$

In the context of this investigation, the term "n" refers to the electronic transition, "B" is a parameter that is dependent on the system, and "Eg" stands for the optical band gap. The value of n can be either 1/2, 2, 3/2, or 3 [14]. Based on Figure 3, the optical band gap values for 0.98 ($NaNbO_3$) -0.02 $Bi_{0.45}Gd_{0.05}K_{0.5}Zr_{0.7}Ti_{0.3}O_3$ and 0.85 ($NaNbO_3$) -0.15$Bi_{0.45}Y_{0.04}K_{0.5}Zr_{0.7}Ti_{0.3}O_3$ are 3.29 eV and 2.8 eV, respectively, which show the energy. The energy gap values of the $NaNbO_3$ compounds with BY/GdKZ substitutions have changed, meaning the material's electronic structure has also changed.

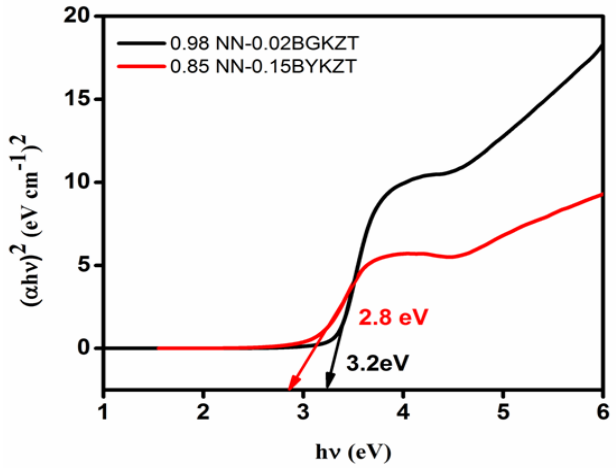

Figure 3: Raman spectrum of $BiGd/YKZTO_3$ Doped $NaNbO_3$

FE-SEM: The Field Emission Scanning Electron Microscope (FE-SEM) is a powerful tool used for the detailed analysis of the morphology of materials such as 0.98 ($NaNbO_3$)-0.02 $Bi_{0.45}Gd_{0.05}K_{0.5}Zr_{0.7}Ti_{0.3}O_3$and 0.85 ($NaNbO_3$)-0.15 $Bi_{0.45}Y_{0.04}K_{0.5}Zr_{0.7}Ti_{0.3}O_3$ at exceptionally high magnifications. The images captured in Figure 4 (a–b) provide a visual representation of these materials' grain size and surface characteristics, offering valuable insights into their structural properties.

The FESEM images of the pelletized materials depicted in Figure 4 (a-b) not only showcase the morphology observations drawn from the micrographs but indicate that the Gd and Y doped samples exhibit crystallization in the micrometre size range, showcasing excellent crystalline characteristics [11]-[13]. Both materials exhibit unidirectional grain growth, with Gd-doped materials showing higher directional alignment than their Y-doped counterparts. As the doping concentration of BYKZT increases and the sample density rises, there is a noticeable difference between the BGKZT samples and BYKZT-doped materials.

.

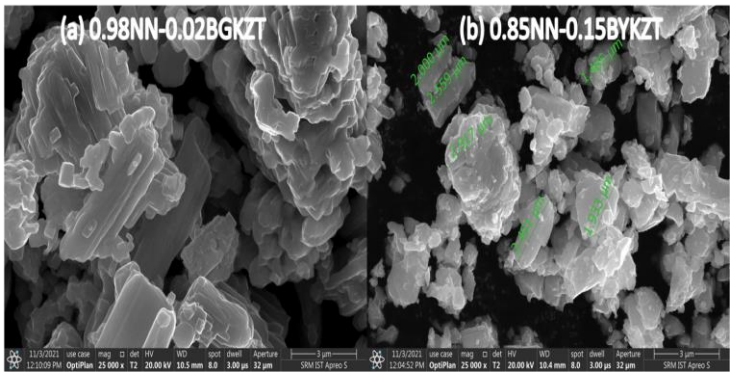

Figure 4: (a) & (b) Raman spectrum of $BiGd/YKZTO_3$ Doped $NaNbO_3$

There is a good chance that this is happening because too many Zr^{4+} and Bi^{3+} ions are building up at the edges of the grains, stopping them from growing further. This hypothesis sheds light on the differing growth patterns observed in Gd and Y-doped materials, highlighting the intricate interplay of dopant concentrations and material density in shaping the morphology of these complex compositions.

Dielectric constant: In Figure 5 (a and c), we measured the temperature-dependent dielectric constant between 100 and 500 °C for 0.98 ($NaNbO_3$)-0.02 $Bi_{0.45}Gd_{0.05}K_{0.5}Zr_{0.7}Ti_{0.3}O_3$ and 0.85 ($NaNbO_3$)-0.15 $Bi_{0.45}Y_{0.04}K_{0.5}Zr_{0.7}Ti_{0.3}O_3$. We may detect anomaly peaks when we heat the ceramics in this temperature range at frequencies between 10 kHz and 1 MHz. As the amount of BYKZT and BGKZT doping increases, the dielectric constant and loss increase peaks get closer to temperatures of more than 300 °C. The Curie temperature transition (Tc) between 300°C and 400°C depends on the doping of Y and Gd, as does the transition from ferroelectric (FE) to antiferroelectric (AFE) states at temperatures between 240°C and 300°C [15]-[16]. However, doping with Gd decreased the Curie temperature. This section primarily discusses the relationship between the quantity of $BiYKZrO_3$ and the Curie temperature (Tc), which decreases from over 300 °C to below 400 °C.

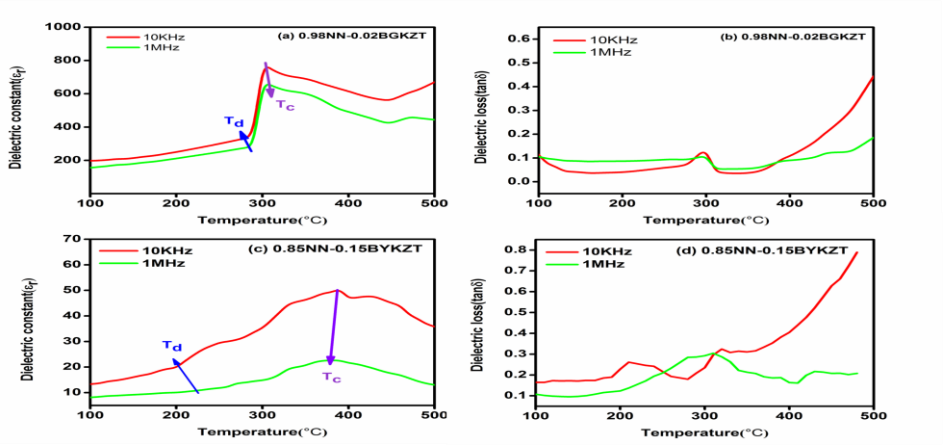

Figure 5: The dielectric constant of $BiGd/YKZTO_3$ Doped $NaNbO_3$ (b and d) Dielectric loss.

In Figure 5 (b and d), we measured the temperature-dependent dielectric loss between 100 and 500 °C for 0.98 ($NaNbO_3$)-0.02 $Bi_{0.45}Gd_{0.05}K_{0.5}Zr_{0.7}Ti_{0.3}O_3$ and 0.85 ($NaNbO_3$)-0.15 $Bi_{0.45}Y_{0.04}K_{0.5}Zr_{0.7}Ti_{0.3}O_3$. The results showed that the dielectric loss of 0.98 ($NaNbO_3$)-0.02 $Bi_{0.45}Gd_{0.05}K_{0.5}Zr_{0.7}Ti_{0.3}O_3$ was less than 0.85 ($NaNbO_3$)-0.15 $Bi_{0.45}Y_{0.04}K_{0.5}Zr_{0.7}Ti_{0.3}O_3$, which means that the first composition is more stable at high temperatures. The results show that the 0.98 ($NaNbO_3$)-0.02 $Bi_{0.45}Gd_{0.05}K_{0.5}Zr_{0.7}Ti_{0.3}O_3$ material might be useful in high-temperature settings where low dielectric loss is important for performance and dependability.

6. Discussion

6.1. Analysis of the emission spectrum

We can see in Figure 6 how the 0.98 ($NaNbO_3$)-0.02 $Bi_{0.45}Gd_{0.05}K_{0.5}Zr_{0.7}Ti_{0.3}O_3$ and 0.85 ($NaNbO_3$)-0.15 $Bi_{0.45}Y_{0.04}K_{0.5}Zr_{0.7}Ti_{0.3}O_3$ monitors give off light when a 422nm laser shines on them with different amounts of BiY/GdKZrTiO_3 ions. The emission bands observed in the spectra of the studied materials are centered around 522 nm (green), 575 nm (yellow), and 693 nm (red). These emissions are primarily attributed to the lattice-sensitized mechanism, where the oxides in Y_2O_3 and Gd_2O_3 contribute to the formation of different Bi^{3+} centers that act as luminescent sites. The luminescence is a result of processes involving bismuth (Bi) and sodium niobate ($NaNbO_3$), which interact to quench the triplet luminescence of these Bi^{3+} centers at low temperatures. This quenching process effectively leads to the observed emissions in the visible spectrum, making these materials promising for applications in optoelectronic devices.

The materials' luminescent properties are significantly influenced by the presence of lanthanides, a group of elements that occupy a unique position in the periodic table. Lanthanides range from lanthanum (La, Z = 57) to lutetium (Lu, Z = 71). However, elements like yttrium (Y, Z = 39) and scandium (Sc, Z = 21) are sometimes included due to their chemical similarities to lanthanides. The electronic structure of these elements is characterized by the filling of the 4F orbitals, with cerium (Ce, Z = 58, configuration $4F^1$) marking the beginning and lutetium (Lu, Z = 71, configuration $4F^{14}$) the completion of this electron shell.

In crystalline or amorphous matrices, lanthanides typically exist in a trivalent state (Ln^{3+}), though divalent states (Ln^{2+}) can occasionally occur under certain conditions. The trivalent state is favored due to the stability provided by the partially filled 4F orbitals, which are shielded from the environment by the outer $5S^2$ and $5P^6$ orbitals. This unique electronic configuration allows lanthanides to exhibit sharp and well-defined emission lines, which are valuable in various applications, including lighting, displays, and phosphors.

When incorporated into a host matrix, the specific luminescent properties of lanthanides depend on their interaction with the surrounding lattice, which can influence the energy levels and transitions of the 4F electrons. This interaction, combined with the lattice structure of the host material, determines the efficiency and wavelength of the emitted light, making lanthanide-doped materials highly versatile for use in photonic devices.

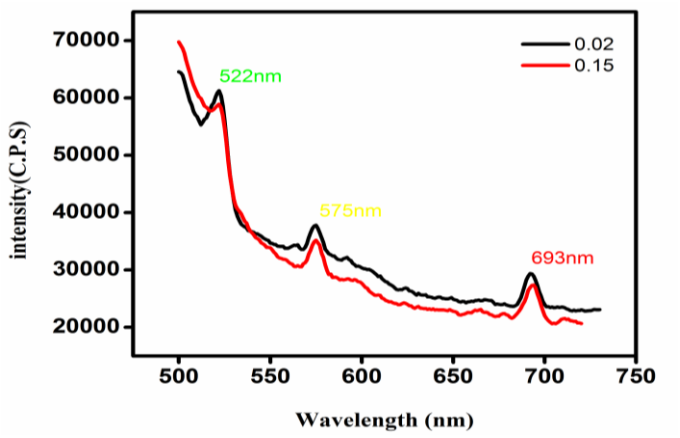

Figure 6: the emission spectrum of BiGd/YKZTO_3 Doped $NaNbO_3$

All three-valent lanthanide ions glow brightly in a narrow band in various host materials. This is because they go through intra-configurationally 4f-4f transitions. Lanthanide ions in solid hosts have radiative transitions that are the same as those of free ions. This is because the 5s2 and 5p6 electrons protect the 4f shells very well. The electrical configuration of the neutral elements in lanthanides is [Xe] $4f^{N-1}$ 5d $6S^2$ [18].

6.2. Ferroelectric

When varying amounts of BY/GdKZT are added to $NaNbO_3$, the P-E hysteresis loops can be seen in Figure 7(a–b). All samples were subjected to an electric field ranging from 18 to 25 kV/cm at room temperature.

Ceramics containing 0.98 ($NaNbO_3$)-0.02 $Bi_{0.45}Gd_{0.05}K_{0.5}Zr_{0.7}Ti_{0.3}O_3$ and 0.85 ($NaNbO_3$)-0.15 $Bi_{0.45}Y_{0.04}K_{0.5}Zr_{0.7}Ti_{0.3}O_3$ showed a high maximum polarization value in Y-doped materials. However, the 0.85NN-0.15BYKZT material displayed a leakage loop, indicating the presence of defects or impurities that impacted its behaviour. Further analysis is needed to understand the origin and effect of these defects on the material's performance. The study demonstrated that adding yttrium to ($NaNbO_3$)-$Bi_{0.45}Gd_{0.05}K_{0.5}Zr_{0.7}Ti_{0.3}O_3$ ceramics improved their ferroelectric properties, making them suitable for electric fields. However, the defects in the 0.85NN-0.15BYKZT material underscore the need for additional research to optimize its performance. Investigating the origin of these defects can help improve the material's properties and fully utilize its potential in various technological applications.

On the other hand, the 0.98NN-0.02BYKZT ceramic exhibited a high maximum polarization value, indicating promising potential for applications requiring strong ferroelectric properties. The different concentrations of BYKZT in $NaNbO_3$ ceramics offer a range of possibilities for customizing their electrical properties to meet specific technological needs. With further experimentation and analysis, scientists may be able to adjust the composition of the 0.98NN-0.02BYKZT ceramic to enhance its ferroelectric properties further. This could lead to new applications in advanced electronic devices or energy storage systems. In summary, the versatility and adjustability of these ceramics make them a valuable material for future technological advancements.

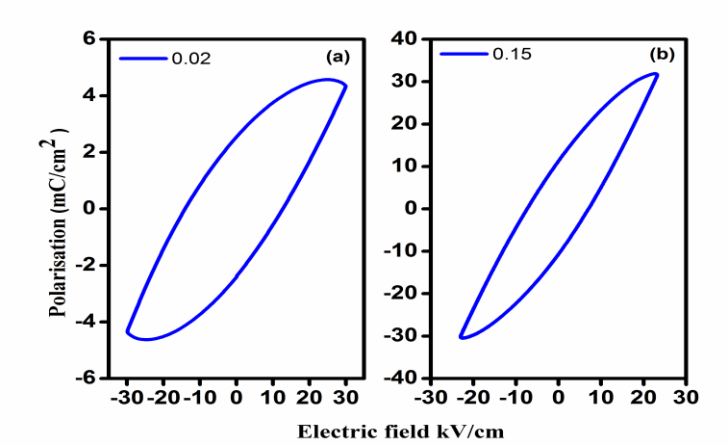

Figure 7: (a) the emission spectrum of $BiGdKZTO_3$ Doped $NaNbO_3$ (b) (a) the emission spectrum of $BiYKZTO_3$ Doped $NaNbO_3$

6.3. Piezoelectric

The study found that two ceramic compositions, 0.98 ($NaNbO_3$)-0.02 $Bi_{0.45}Gd_{0.05}K_{0.5}Zr_{0.7}Ti_{0.3}O_3$ and 0.85 ($NaNbO_3$)-0.15 $Bi_{0.45}Y_{0.04}K0.5Zr_{0.7}Ti_{0.3}O_3$ exhibit piezoelectric properties at room temperature. The piezoelectric coefficients (d_{33}) were observed to be the piezoelectric constant, which ranged between 150 and 250 pC/N. Both compositions showed a better piezoelectric response after poling at 2.5 KV/cm for two hours, with the d_{33} values reaching their highest at this voltage level. This implies that the poling process plays a crucial role in enhancing the piezoelectric response of the materials.

The study also suggested that the composition of the ceramics affects their piezoelectric properties. The 0.85 ($NaNbO_3$)-0.15 $Bi_{0.45}Y_{0.04}K_{0.5}Zr_{0.7}Ti_{0.3}O_3$ mixture had a higher piezoelectric constant of 250 pC/N, which means it worked better as a piezoelectric material than the other mixture.

Moreover, the piezoelectric properties of the ceramics were influenced by the grain size and porosity of the materials. A smaller grain size and lower porosity resulted in higher piezoelectric constants, highlighting the role of microstructure in determining their performance. This suggests that optimizing the microstructure of these materials could lead to even greater improvements in their piezoelectric properties. Also, figuring out the basic rules that control how these ceramics behave piezoelectrically could help make new and better piezoelectric materials that can be used in various situations (Figure 8).

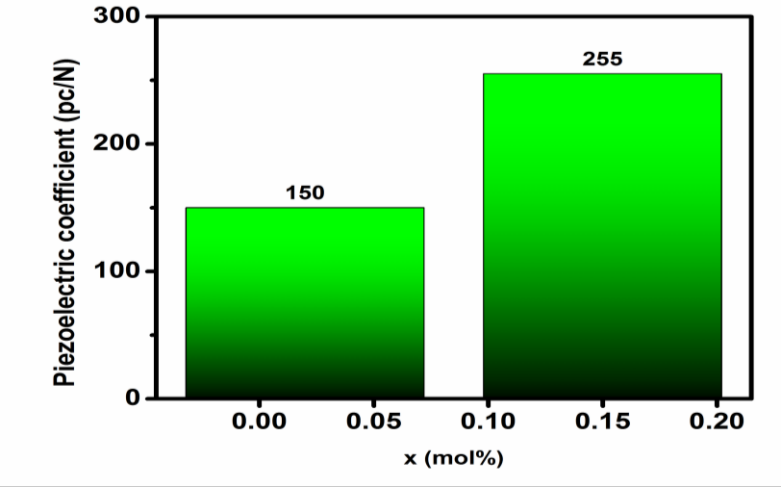

Figure 8: The piezoelectric coefficients of $BiGdKZTO_3$ and $BiYKZTO_3$ Doped $NaNbO_3$

7. Conclusion

The novel ceramic composites are 0.98 ($NaNbO_3$)-0.02 $Bi_{0.45}Gd_{0.05}K_{0.5}Zr_{0.7}Ti_{0.3}O_3$ and 0.85-0.15 $Bi_{0.45}Y_{0.04}K_{0.5}Zr_{0.7}Ti_{0.3}O_3$. Lead-free and polycrystalline were made using the solid-state method and using two-step sintering. In this study, a Pmc21 and Pbma: bca space group perovskite structure was identified in the material, indicating a complex and ordered crystal structure. The particle size and strain were calculated from XRD spectra using the Scherrer formula and Williamson-Hall method, revealing detailed insights into the material's microstructure. Raman spectroscopy demonstrated a decrease in vibrational spectral line frequency between 100 and 800 cm^{-1}, suggesting alterations in the material's lattice dynamics. FE-SEM images further corroborated this by showing distinct and varied grain morphology, highlighting the influence of processing conditions on microstructural development. UV-Vis spectra analysis revealed band gap values ranging from 3.2 to 2.8 eV, which are critical for understanding the material's electronic properties. Photoluminescence spectra exhibited emission bands at 522 nm (green), 575 nm (yellow), and 693 nm (red), indicating the material's potential for optoelectronic applications. Dielectric measurements between 10 kHz and 1 MHz revealed weaker dielectric symmetry, which may be linked to the material's inherent structural characteristics. Furthermore, increased doping significantly enhanced the ferroelectric and piezoelectric coefficients, with d33 values reaching 150 and 255 pC/N, respectively. These findings suggest that the material holds promise for advanced piezoelectric applications, with its properties tunable through doping and processing.

Acknowledgement: We acknowledge the Nanotechnology Research Centre (NRC) and SRM IST for their support in conducting the XRD, UV, Raman, FE-SEM, and electrical studies.

Data Availability Statement: The data for this study can be made available upon request to the corresponding author.

Funding Statement: This manuscript and research paper were prepared without any financial support or funding

Conflicts of Interest Statement: The authors declare no conflicts of interest. This work is original, with all citations and references properly included.

Ethics and Consent Statement: This research follows ethical guidelines, with informed consent obtained and confidentiality ensured.

References

1. N. M. J. Haun, E. Furman, S. J. Jang, H. A. McKinstry, and L. E. Cross, “Thermodynamic theory of PbTiO3,” J. Appl. Phys., vol. 62, no. 8, pp. 3331–3338, 1987.
2. Q. Zhang et al., “Ti x) O 3 antiferroelectric ceramics under DC bias field,” Appl. Phys. A, vol. 103, no.4, pp. 1159–1163, 2011.

3. N. H. Hussin, M. F. M. Taib, O. H. Hassan, M. Z. A. Yahya, and R. Zakaria, “Study of geometrical and electronic structure of lanthanum doped PbTiO3 and PbZrTiO3: First principles calculation,”. vol.2030, no.1, pp. 020032, 2018.
4. W. Liang, W. Wu, D. Xiao, and J. Zhu, Effect of the addition of CaZrO3 and LiNbO3 on the phase transitions and piezoelectric properties of K0. 5Na0. 5NbO3 lead-free ceramics,” Am. Ceram. Soc, vol. 94, no.12, pp. 4317–4322, 2011.
5. G. K. L. Goh, F. F. Lange, S. M. Haile, and C. G. Levi, “Hydrothermal synthesis of KNbO3 and NaNbO3 powders,” J. Mater. Res., vol. 18, no. 2, pp. 338–345, 2003.
6. B. Malic, D. Jenko, J. Bernard, J. Cilensek, and M. Kosec, “Synthesis and sintering of (K, Na) NbO3 based ceramics,” Mater Res Soc Symp Proc (OPL), vol. 755, no.2, pp. D4-4, 2002.
7. W. Bai et al., “NaNbO3 templates-induced phase evolution and enhancement of electromechanical properties in grain oriented lead-free BNT-based piezoelectric materials,” J. Eur. Ceram. Soc, vol. 37, no.7, pp. 2591–2604, 2017.
8. M. Nižňanský, K. Vanmeensel, J. Vleugels, V. Tyrpekl, and M. Vilémová, “Review on high-pressure spark plasma sintering and simulation of the impact of die/punch material combinations on the sample temperature homogeneity,” Open Ceramics, vol. 16, no.1, p-100433, 2023.
9. O. Guillon et al., “Field-assisted sintering technology/spark plasma sintering: Mechanisms, materials, and technology developments: FAST/SPS: Mechanisms, materials, and technology developments,” Adv. Eng. Mater., vol. 16, no. 7, pp- 830–849, 2014.
10. D. Lin et al., “High rhombohedral to tetragonal phase transition temperature and electromechanical response in Pb (Yb1/2Nb1/2) O3-Pb (Sc1/2Nb1/2) O3-PbTiO3 ferroelectric system near the morphotropic phase boundary,” Journal of the European Ceramic Society, vol. 39, no.6, pp.2082–2090, 2019.
11. P. Elaiyaraja and N. Karunagaran, “An orthorhombic pseudo-cubic phase transition by approaching the Landau symmetrical impact of piezoelectric and ferroelectric properties in novel NaNbO3-based solid solutions,” J. Mater. Sci. Res, vol. 38, no.2, pp.2463–2473, 2023.
12. P. Elaiyaraja, and N. Karunagaran. "The efficacy of Bi0. 46Y0. 04K0. 5ZrO3 doped three-step sintering to accomplish high piezoelectric and ferroelectric properties in new lead-free NaNbO3-based materials." Ceram. Int. vol.50, no.3, pp. 4810-4822, 2024.
13. P. Elaiyaraja and N. Karunagaran. "Exploring the possibilities of lead-free 0.98 NaNbO3-0.02 BiSmKZrO3 for electrical and optical applications using solid-state method." Mater. Sci. Semicond. Process. vol. 172, no.2, p.108053, 2024.
14. G. Sudha, P. Elaiyaraja, and N. Karunagaran. "Correlation between structural, luminescence, and dielectric properties of novel Sm3+ and trioxotungsten-doped NBBT ceramic system for multifunctional device applications." J. Mater. Sci.: Mater. Electron. Vol. 33, no. 34, pp. 25532-25550, 2022.
15. X. Hao, J. Zhai, L. B. Kong, and Z. Xu, “A comprehensive review on the progress of lead zirconate-based antiferroelectric materials,” Prog. Mater. Sci., vol. 63, no.6, pp. 1–57, 2014.
16. F. Ali et al., “Recent progress on energy-related applications of HfO2-based ferroelectric and antiferroelectric materials,” ACS Appl. Electron. Mater, vol. 2, no.7, pp. 2301–2317, 2020.
17. S. G. Semenov, M. E. Bedrina, A. E. Buzin, and A. V. Titov, “Structural parameters and electron transfer in ytterbium, lutetium, and cerium compounds with hydrocarbon monocycles,” Russ. J. Gen. Chem., vol. 89, no. 7, pp.1424–1432, 2019.
18. A. Soni and B. P. Kumar, “Luminescent materials in lighting, display, solar cell, sensing, and biomedical applications,” in Luminescence-OLED Technology and Applications, London, UK: IntechOpen, pp. 1-23,2019.